

Effect of optical purity on phase sequence in antiferroelectric liquid crystals

Nataša Vaupotič^{1,2} and Mojca Čepič^{1,3}

¹Institut Jozef Stefan, Ljubljana, Slovenia

²Department of Physics, Faculty of Education, University of Maribor, Maribor, Slovenia

³Department of Physics, Faculty of Education, University of Ljubljana, Maribor, Slovenia

October 21, 2018

Abstract

We use the discrete phenomenological model to study theoretically the phase diagrams in antiferroelectric liquid crystals (AFLCs) as a function of optical purity and temperature. Recent experiments have shown that in some systems the number of phases is reduced if the optical purity is extremely high. In some materials the SmC_A^* phase is the only stable tilted smectic phase in the pure sample. In the scope of the presented model this high sensitivity of the phase sequence in the AFLCs to optical purity is attributed to the piezoelectric coupling which is reduced if optical purity is reduced. We limit our study to three topologically equal phases - SmC^* , SmC_α^* and SmC_A^* and show that the reduction of optical purity forces the system from the antiferroelectric to the ferroelectric phase with a possible SmC_α^* between them. The effect of the flexoelectric and quadrupolar coupling is considered as well. If the phase diagram includes only two phases, SmC^* and SmC_A^* , the flexoelectric coupling is very small. The materials which exhibit the SmC_α^* in a certain range of optical purity and temperature, can be expected to have a significant flexoelectric coupling that is comparable with the piezoelectric coupling. And finally, when temperature is lowered the phase sequence $\text{SmA} \rightarrow \text{SmC}_\alpha^* \rightarrow \text{SmC}^* \rightarrow \text{SmC}_A^*$ is possible only in materials in which quadrupolar coupling is very strong.

1 Introduction

Antiferroelectric liquid crystals (AFLCs) were discovered more than 15 years ago when macroscopic properties of mixtures of left- and right-handed MH-POBC, nowadays known as a prototype antiferroelectric liquid crystal, were studied [1]. Scientists were surprised at the rich variety of phases found in these systems and at the influence that the optical purity has on the phase sequence. There is a number of phenomena found in these complex systems [2]-[6] and the macroscopic properties of some of the phases were explained only recently by the theoretical modelling of the microscopic structure [7].

In chiral antiferroelectric liquid crystals there always exists at least one phase with antiferroelectric properties, the SmC_A^* phase [5]. Due to the oppositely (anticlinically) tilted elongated molecules in the neighboring layers, the piezoelectrically induced polarization is cancelled out and the system behaves antiferroelectrically in the external electric field. The structure is additionally helicoidally modulated by a double helix formed from anticlinically tilted layers. The length of the pitch depends on optical purity and it is infinite in racemic mixtures. The synclinically tilted ferroelectric SmC^* phase is also often found in AFLCs. It is stable at higher temperatures than the SmC_A^* phase. In the temperature range between the SmC_A^* and the SmC^* phase two other phases with a short modulation over 3 and 4 layers and long helicoidal modulation over at least few hundred of layers can exist [6]. They are called $\text{SmC}_{FI,I}^*$ and $\text{SmC}_{FI,II}^*$, respectively. In optically very pure samples the 4-layer phase is sometimes stable within the same temperature range as the SmC^* phase [8]. Directly below the transition to the tilted phase, the phase called SmC_α^* can be stable. This phase is topologically equal to the SmC^* phase but the period of the helicoidal modulation extends over a few layers only. The phase transition between the SmC_α^* and SmC^* is of an isostructural type and can be recognized by differential calorimetry measurements only if the changes of the properties like the length of the modulation period or the tilt magnitude is abrupt [9]. More exact measurements like simultaneous measurements of optical rotatory power and the tilt [10] have shown that the phase exist also at lower optical purities but transforms continuously to the structure of the SmC^* phase with a very rapid changes of modulation period within an extremely narrow temperature range (a few mK) [11].

Optical purity has a strong influence on the phase sequence. It was generally believed that the number of phases increases with increasing the optical purity. However, recent experiments [12, 13] has shown that in some systems

the opposite is true, i.e. the number of phases is reduced if the optical purity is extremely high. In some materials the SmC_A^* phase is the only stable tilted smectic phase in the pure sample.

The motivation of this work was to account for the described properties of the phase diagram of antiferroelectric liquid crystals within the framework of the discrete phenomenological model. We limit our consideration to the phase diagram of three topologically equal phases, also called the clock phases - SmC^* , SmC_α^* and SmC_A^* , that all have helicoidally modulated structures with pitches of a few hundred layers, of a few layers, and of approximately two layers, respectively. All three phases may appear directly below the non-tilted SmA phase. Experimentally three different phase diagrams have been observed [12], which are presented schematically in Fig. 1. This high sensitivity of AFLCs to optical purity has so far been attributed to changes in smectic order [13]. The aim of our study is to show that chiral microscopic interactions might also be responsible for the observed macroscopic behavior. The plan of the paper is the following. First we present the discrete phenomenological model and discuss the theoretical predictions on how optical purity affects the phase sequences. Then we present theoretically obtained phase diagrams in which stability regions of phases are shown as a function of temperature and optical purity. Finally we discuss the results and draw the conclusions.

2 Model

We use the discrete phenomenological model [14] and write the free energy of the system in terms of the tilt vector $\boldsymbol{\xi}_j$ and the polar order parameter $\boldsymbol{\eta}_j$ (see Fig. 2) in the j -th smectic layer. The tilt vector is the projection of the director \mathbf{n} to the smectic plane and its magnitude is equal to the tilt ϑ . The spontaneous polarization in the j -th layer is proportional to the polar order parameter: $\mathbf{P}_j = P_0 \boldsymbol{\eta}_j$, where P_0 is the polarization of the completely polarly ordered layer [15]. Because of that the polar order parameter will be referred to as *polarization*.

The free energy of the smectic system with N layers is:

$$\begin{aligned} G = & a \sum_{j=1}^N \frac{1}{2} (T - T_0) \boldsymbol{\xi}_j^2 + \frac{1}{4} b \boldsymbol{\xi}_j^4 + \frac{1}{2} a_{10} (\boldsymbol{\xi}_j \cdot \boldsymbol{\xi}_{j+1}) + \frac{1}{2} a_{11} \boldsymbol{\xi}_j^2 (\boldsymbol{\xi}_j \cdot \boldsymbol{\xi}_{j+1}) \\ & + \frac{1}{2} f_1 (\boldsymbol{\xi}_j \times \boldsymbol{\xi}_{j+1})_z + \frac{1}{2} b_0 \boldsymbol{\eta}_j^2 + \frac{1}{2} b_1 (\boldsymbol{\eta}_j \cdot \boldsymbol{\eta}_{j+1}) + \frac{1}{8} b_2 (\boldsymbol{\eta}_j \cdot \boldsymbol{\eta}_{j+2}) \end{aligned}$$

$$+c_p (\boldsymbol{\eta}_j \times \boldsymbol{\xi}_j)_z + \frac{1}{2}\mu (\boldsymbol{\xi}_{j-1} - \boldsymbol{\xi}_{j+1}) \cdot \boldsymbol{\eta}_j + \frac{1}{2}b_Q (\boldsymbol{\xi}_j \cdot \boldsymbol{\xi}_{j+1})^2 . \quad (1)$$

The significance of the parameters entering the model is discussed in detail elsewhere [7, 14], so we make only a short review. The first two terms describe the intralayer steric and the attractive van der Waals interactions. The phase transition to the tilted phase in an isolated layer occurs at temperature T_0 . The parameters a_{10} and f_1 give the achiral and the chiral part of the van der Waals interaction between the nearest layers. The fourth term in Eq.(1) describes the variation of the achiral van der Waals interaction with temperature. The parameter a_{11} is negative to account for the fact that with reduced temperature (and thus increased tilt) the antiferroelectric liquid crystal is always driven to the SmC_A^* phase. The parameters b_0 , b_1 and b_2 give the electrostatic interaction inside the layer, between the nearest layers and the next nearest layers, respectively. It was shown [16] that the electrostatic interaction between the next nearest layers does not significantly affect the structure, therefore in the rest of the paper we set $b_2 = 0$. The magnitude of the piezoelectric coupling between the tilt and the polarization is given by c_p and the flexoelectric coupling, i. e. the coupling between the variation of the tilt and the polarization, is given by the parameter μ . The quadrupolar coupling (b_Q) favors both synclinic and anticlinic ordering in the neighboring layers [17, 18], so b_Q is negative. All the parameters are given in the units of K, except the parameter a , which has the unit $\text{Jm}^{-3}\text{K}^{-1}$.

In this paper we focus only on the clock structures where the polarization ($\boldsymbol{\eta}_j$) is perpendicular to the tilt vector and the angle between the tilt vectors in the neighboring layers is constant and equal to α . When the free energy (Eq. (1)) is minimized with respect to the magnitude of the polar order parameter η , we find:

$$\eta = \frac{(c_p - \mu \sin \alpha) \vartheta}{b_0 + b_1 \cos \alpha} . \quad (2)$$

The polarization inside one layer thus increases with increasing tilt and as a result the importance of electrostatic interaction increases when temperature is reduced. The polarization, however, increases also if the piezoelectric coupling (c_p) between the neighboring layers increases. The amount of piezoelectric coupling strongly depends on the optical purity of the sample. The parameter x is chosen as a measure for optical purity. In pure samples $x = 1$ and in a racemized sample $x = 0$. The piezoelectric parameter can then be written as $c_p = xc_{p0}$. The inlayer polarization (Eq. (2)) thus decreases with

decreasing optical purity which suggests that materials which exhibit antiferroelectric structure at high optical purity might be in the ferroelectric state at low optical purity. Changes in optical purity affect also the chiral part of the van der Waals interaction (f_1) which can be rewritten as $f_1 = xf_{10}$.

Elimination of the polar order parameter from Eq. (1) leads to the free energy expressed only in tilt vectors:

$$\begin{aligned} G/a = & \sum_{j=1}^N \frac{1}{2}(T - T_0)\boldsymbol{\xi}_j^2 + \frac{1}{4}b\boldsymbol{\xi}_j^4 + \frac{1}{2}a_{11}\boldsymbol{\xi}_j^2(\boldsymbol{\xi}_j \cdot \boldsymbol{\xi}_{j+1}) + \frac{1}{2}b_Q(\boldsymbol{\xi}_j \cdot \boldsymbol{\xi}_{j+1})^2 \\ & + \frac{1}{2} \sum_{i=1}^4 \tilde{a}_i(\boldsymbol{\xi}_j \cdot \boldsymbol{\xi}_{j+i}) + \frac{1}{2} \sum_{i=1}^3 \tilde{f}_i(\boldsymbol{\xi}_j \times \boldsymbol{\xi}_{j+i})_z . \end{aligned}$$

The electrostatic interaction mediates the indirect interaction among the layers which extends up to the fourth-nearest layer. The whole set of effective achiral (\tilde{a}_i) and chiral (\tilde{f}_i) parameters is given in [14]. The effective parameters between the nearest and the next nearest layers determine the type of the clock phase (SmC_α^* , SmC_A^* or SmC^*). The interactions up to the third and the fourth nearest layers are important only when phases with a short modulation over three and four layers need to be considered. Although in the numerical calculations we have included the whole set of the effective parameters, we have checked that \tilde{a}_3 , \tilde{a}_4 and \tilde{f}_3 actually have no influence on the phase diagrams. Because of that we discuss in more detail only the effective parameters between the nearest and the next-nearest neighboring layers:

$$\tilde{a}_1 = a_{10} + \left(\frac{c_p^2}{b_0} + \frac{\mu^2}{4b_0} \right) \frac{b_1}{b_0} , \quad (3)$$

$$\tilde{a}_2 = -\frac{c_p^2}{2b_0} \frac{b_1^2}{b_0^2} + \frac{\mu^2}{2b_0} , \quad (4)$$

$$\tilde{f}_1 = f_1 + \frac{2c_p\mu}{b_0} \left(1 + \frac{b_1^2}{4b_0^2} \right) , \quad (5)$$

$$\tilde{f}_2 = -\frac{c_p\mu}{b_0} \frac{b_1}{b_0} . \quad (6)$$

The type of the structure (SmC^* or SmC_A^*) depends mainly on the sign and the magnitude of the parameter \tilde{a}_1 . If it is negative, synclinic ordering between the neighboring layers is favored, and anticlinic ordering is favored

if it is positive. The second term in \tilde{a}_1 (see Eq. (3)) is always positive and its magnitude increases if c_p increases. So, if the direct achiral part of the van der Waals interaction between the nearest layers is such that it favors synclinic ordering in the neighboring layers ($a_{10} < 0$) the net effect of all interactions (described by \tilde{a}_1) might be such that the anticlinic ordering between the nearest layers is preferred, providing that the effect of piezo- and flexoelectric coupling (the second term in \tilde{a}_1 (see Eq. (3))) is large enough to overrun the direct van der Waals interaction. This means, that in materials in which c_{p0} is large compared to a_{10} one can expect that the reduction of optical purity will drive the material from the antiferroelectric to the ferroelectric state.

In materials where the effective achiral interaction between the next-nearest layers (\tilde{a}_2) is positive, this interaction favors anticlinic ordering between the next nearest layers. This ordering is in contradiction with both the synclinic and the anticlinic ordering in the nearest layers and it enforces the stability of the SmC_α^* phase if the condition $4|\tilde{a}_1| < \tilde{a}_2$ is satisfied [14]. If upon reduction of the optical purity the effective achiral interaction between the nearest layers changes sign, the stability condition for the SmC_α^* phase is bound to be satisfied in a certain range of optical purity and the following phase sequence can be observed when optical purity is reduced: $\text{SmC}_A^* \rightarrow \text{SmC}_\alpha^* \rightarrow \text{SmC}^*$.

3 Theoretical Phase Diagrams

The aim of this work was to obtain theoretically the phase diagrams that qualitatively agree with the experimental phase diagrams, shown in Fig. 1. Following that goal we use the model presented above and discuss the effect that the change in chiral microscopic interactions has on the phase diagram. In addition we also discuss the effect of the quadrupolar and the flexoelectric coupling. Finally we show that by looking at the certain characteristics of the experimental phase diagram one can predict which macroscopic interactions are most important in a given material.

First we focus on the effect of the piezoelectric coupling (c_p) and set the flexoelectric (μ) and the quadrupolar coupling (b_Q) to zero. In this case only three effective interlayer parameters ($\tilde{a}_1 = a_{10} + c_p^2 b_1 / b_0^2$, $\tilde{a}_2 = -c_p^2 b_1^2 / (2b_0^3)$ and $\tilde{f}_1 = f_{10}x$) are different from zero. There is no frustration between the nearest and the next nearest layer interactions (\tilde{a}_2 is negative) so a very simple phase

diagram, containing only the SmC_A^* phase and the SmC^* phase, is expected. When the chiral part (f_{10}) of the van der Waals interaction is very small the phase diagram is indeed simple (see Fig. 3a). This diagram qualitatively agrees with the phase diagram in Fig. 1a. However, if the chiral part of the van der Waals interaction (f_{10}) is increased, the helicoidal modulation can become so large, that the structure might be recognized as the SmC_α^* phase. The phase angle increases continuously when temperature is lowered. In Fig. 3a we have shown the region of optical purity and temperature in which the phase angle α is greater than 0.2. This modulation is already so large that the phase might be recognized as the SmC_α^* phase.

Next we include the quadrupolar coupling (b_Q), which tends to stabilize synclinic or anticlinic phases. The presence of small quadrupolar coupling reduces the region of stability of the SmC_α^* phase significantly as seen in Fig. 3b. This phase diagram qualitatively agrees with the phase diagram shown in Fig. 1b. At even larger quadrupolar coupling the SmC^* phase 'grows' into the region of the SmC_α^* phase and the SmC_α^* phase is almost expelled from the phase diagram as seen in Fig. 3b.

The diagrams shown in Fig. 3 can be used to predict how a phase diagram for the material which has larger, or lower piezoelectric coupling looks like. If, for example, the piezoelectric coupling c_{p0} is reduced by a factor of 1.5, the new phase diagram would be obtained by a simple rescaling of the optical purity x , which should be multiplied by the same factor, i.e. by 1.5. So, in this case the region of stability of the SmC^* phase would extend to higher optical purity, in the chosen example to $x > 1$. In the case of the very strong quadrupolar coupling the rescaled phase diagram of Fig. 3b qualitatively agrees with the phase diagram in Fig. 1c.

Let us emphasize that when the flexoelectric coupling is negligibly small the SmC_α^* phase is obtained solely due to the strong chiral twist which results from the chiral part of the van der Waals interaction. We believe, however, that the true origin of the SmC_α^* phase is in the frustration between the nearest and the next nearest layer achiral interactions ($\tilde{a}_2 > 0$). This frustration is possible only in materials in which flexoelectric coupling (μ) is important. So in the rest of the Section we discuss the effect of the flexoelectric coupling in more detail.

The flexoelectric coupling has several effects. As already mentioned it changes the effective interaction between the next nearest layers (see Eq. (4)) so that anticlinic ordering is preferred ($\tilde{a}_2 > 0$). It is also important that at $\mu \neq 0$ the effective chiral interactions up to the second (see Eq. (6))

and the third nearest layers are present. This interactions have a significant effect on the magnitude of the phase angle α . It is shown below that when the effective chiral interactions between the nearest and the next nearest layers are opposing each other the region of stability of the SmC_α^* phase is significantly reduced compared to the case where \tilde{f}_1 and \tilde{f}_2 have the same sign. At fixed flexo (μ), piezo (c_{p0}) and electrostatic (b_0 , b_1) interactions the sign of the effective chiral parameter \tilde{f}_1 depends on the magnitude of the direct chiral van der Waals interaction (f_{10}) between the nearest layers (see Eq. (5)). Only minor changes in this interaction can cause a change in the sign of \tilde{f}_1 which then essentially leads to a significant reduction or enlargement of the stability region of the SmC_α^* phase as shown in Fig. 4.

In Fig. 4a,b phase diagrams are shown for materials which differ in the magnitude of the direct chiral van der Waals interaction (f_{10}). In the phase diagram shown in Fig. 4a the effective chiral interactions between the nearest and the next nearest layers prefer the opposite helicoidal modulation and are thus opposing each other. In this case the stability of the SmC_α^* phase is limited to the region of optical purity where the general condition for the stability of the SmC_α^* phase ($4|\tilde{a}_1| < \tilde{a}_2$) is satisfied. If the chiral van der Waals interaction is slightly increased (Fig. 4b) the effective chiral interactions favor the same sense of the helicoidal modulation. So even in the region where the general condition for the stability of the SmC_α^* phase is not satisfied, the helicoidal modulation is so large that the structure might be recognized as the SmC_α^* phase.

In Fig. 4a,b we also show the effect that the increased quadrupolar coupling has on the phase diagram. Since quadrupolar interaction enforces synclinic or anticlinic phases the region of stability of the SmC_α^* phase is reduced. The SmC^* phase is pushed towards higher optical purity and in a certain region of optical purity one obtains the following phase sequence: $\text{SmA} \rightarrow \text{SmC}_\alpha^* \rightarrow \text{SmC}^* \rightarrow \text{SmC}_A^*$ upon lowering the temperature. In the phase diagrams shown in Fig. 4 the phase transitions $\text{SmC}^* \rightarrow \text{SmC}_A^*$ and $\text{SmC}_\alpha^* \rightarrow \text{SmC}_A^*$ are of the first order and the phase transition $\text{SmC}_\alpha^* \rightarrow \text{SmC}^*$ is continuous. However, the type of transition depends strongly on the strength of the piezo and flexoelectric coupling and on the effective chiral interaction between the nearest layers. In Fig. 5 we show the phase diagrams which are obtained if the flexoelectric interaction and the effective chiral interaction are increased and flexoelectric interaction is reduced. At low quadrupolar coupling one can expect the phase diagram shown in Fig. 5a. The phase

transition $\text{SmC}_\alpha^* \rightarrow \text{SmC}_A^*$ has become continuous and the phase transition $\text{SmC}^* \rightarrow \text{SmC}_A^*$ remains first order. Additionally we have a first order transition $\text{SmC}^* \rightarrow \text{SmC}_\alpha^*$ at $0.45 < x < 0.55$. If the quadrupolar coupling is increased the stability region of the SmC^* phase increases on the expense of the SmC_α^* phase (see Fig. 5b). The diagram is similar to the one shown in Fig. 4b, but the phase transition from the SmC_α^* to the SmC^* has become first order. Only in a small range of optical purity the transition is still continuous. The variation of the phase angle with temperature is shown in Fig. 6. At low temperatures tilts in the neighboring layers are anticlinic and slightly distorted from the antiparallel orientation, which is typical for the SmC_A^* phase. Upon heating the structure discontinuously transforms into the synclinic helicoidally modulated structure of the SmC^* phase. Close to the transition temperature to the nontilted phase the phase difference again changes discontinuously and the helicoidally modulated structure with a short pitch, i.e. the SmC_α^* phase, becomes stable.

The phase diagrams shown in Figs. 4,5 are again generic. They can be stretched or compressed in the horizontal direction by a simple rescaling of the piezoelectric parameter c_{p0} and the chiral part of the van der Waals interaction f_{10} . For example, if both parameters are increased by a factor of 1.5, the 'elbow' of the SmC^* phase in Fig. 5b would extend to $x > 1$, which means, that in the optically pure sample ($x = 1$) one would observe the following phase sequence upon lowering the temperature: $\text{SmA} \rightarrow \text{SmC}_\alpha^* \rightarrow \text{SmC}^* \rightarrow \text{SmC}_A^*$ and this would agree with the schematic diagram shown in Fig. 1c. As already mentioned the rescaling of the diagram shown in Fig. 3b also gives a phase diagram which qualitatively agrees with the one on Fig. 1c, however the origin of the SmC_α^* phase in Figs. 3 and 5 is different.

4 Conclusions

The discrete phenomenological model [14] reproduces the general phase diagrams that are consistent with the experimental results [12]. We have shown that the reduction of optical purity, in general, reduces the magnitude of the inlayer polarization which forces the system from the antiferroelectric to the ferroelectric phase with a possible SmC_α^* phase between them.

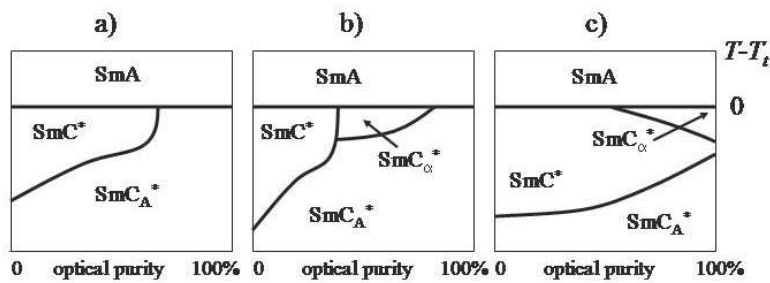
We conclude that from the experimental phase diagrams one can predict the most important microscopic interactions in the material. If the phase diagram includes only two phases, SmC^* and SmC_A^* , the flexoelectric coupling

is very small. The materials which exhibit the SmC_α^* in a certain range of optical purity and temperature, can be expected to have a significant direct chiral van der Waals interaction or/and the flexoelectric coupling that is comparable with the piezoelectric coupling. And finally, when temperature is lowered, the phase sequence $\text{SmA} \rightarrow \text{SmC}_\alpha^* \rightarrow \text{SmC}^* \rightarrow \text{SmC}_A^*$ is possible only in materials in which quadrupolar coupling is very strong. The transitions can be of the first order only if flexoelectric coupling is significant as well. In such materials the phases with a short modulation over three and four layers are usually present as well [7, 12]. The study of these phases, however, is already beyond the scope of this paper.

References

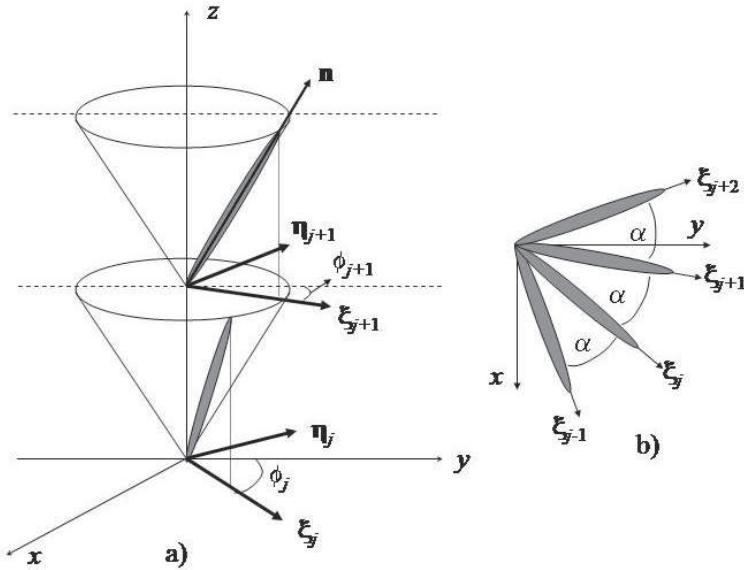
- [1] A. D. L. Chandani, E. Gorecka, Y. Ouchi, H. Takezoe, and A. Fukuda, Jpn. J. Appl. Phys., Part 2 **28**, L1265 (1989); E. Gorecka, A. D. L. Chandani, Y. Ouchi, H. Takezoe, and A. Fukuda, Jap. J. Appl. Phys., Part 1 **29**, 131 (1990).
- [2] Y. Galerne and L. Liebert, Phys. Rev. Lett. **64**, 906 (1990).
- [3] K. Hiraoka, Y. Takanishi, K. Skarp, H. Takezoe, and A. Fukuda, Jap. J. Appl. Phys. **30**, L1819 (1991).
- [4] Ch. Bahr, D. Fliegner, Phys. Rev. Lett. **70**, 1842 (1993).
- [5] A. Fokuda, Y. Takanishi, T. Isozaki, K. Ishikawa, and H. Takezoe, J. Mat. Chem. **4**, 997 (1994).
- [6] P. Mach, R. Pindak, A.-M. Levelut, P. Barois, H. Nguyen, C. Huang, and L. Furenlid, Phys. Rev. Lett. **81**, 1015 (1998).
- [7] M. Čepič, E. Gorecka, D. Pociecha, B. Žekš and H. T. Nguyen, J. Chem. Phys. **117**, 1817 (2002).
- [8] E. Gorecka, D. Pociecha, M. Čepič, B. Žekš, and R. Dabrowski, Phys. Rev. E **65**, 061703 (2002).
- [9] C. W. Garland, Thermochim. Acta **88**, 127 (1985).

- [10] M. Škarabot, M. Čepič, B. Žekš, R. Blinc, G. Heppke, A. V. Kityk, and I. Muševič, Phys. Rev. E **58**, 575 (1998).
- [11] M. Škarabot and I. Muševič, unpublished results
- [12] H. Takezoe, p. 271, in Chirality in Liquid Crystals, Eds. J. Kitzerov and C. Bahr, (Springer, New York, 2001).
- [13] J.P.F. Lagerwall, P. Rudquist, S.T. Lagerwall and F. Giesselmann, Liq. Cryst. **30**, 399 (2003).
- [14] M. Čepič and B. Žekš, Phys. Rev. Lett. **87**, 085501 (2001).
- [15] D. J. Photinos and E. T. Samulski, Science **270**, 783 (1995).
- [16] A. V. Emelyanenko and M. A. Osipov, Phys. Rev. E **68**, 051703 (2003).
- [17] M. P. Neal, A. J. Parker, and C. M. Care, Mol. Phys. **91**, 603 (1997).
- [18] D. Pociecha, E. Gorecka, M. Čepič, N. Vaupotič, B. Žekš, D. Kardas, and J. Mieczkowski, Phys. Rev. Lett. **86**, 3048 (2001).



N. Vaupotic and M. Cepic, Fig. 1

Figure 1: Schematic drawings of the three typical phase diagrams observed in AFLCs. Only the clock structures are shown, the three and four layer phases are omitted. a) TFMHPOBC, b) TFMHPOCBC and c) MHPOBC.



N. Vaupotic and M. Cepic, Fig. 2

Figure 2: The geometry of the problem and the definition of the order parameters. a) Smectic layers run along the z -direction. Molecules lie on the tilt cone, the magnitude of the tilt is ϑ . The system is described by two order parameters: ξ_j and η_j . The tilt vector ξ_j points in the direction of the projection of the director \mathbf{n} to the smectic plane (the xy -plane). Its magnitude is ϑ . The phase angle between the tilt vector in the j -th and the $(j+1)$ -th layer is $\phi_{j+1} - \phi_j = \alpha$ and it is constant. In the SmC^* phase $\alpha \approx 0$ and in the SmC_A^* phase $\alpha \approx \pi$. The polar order parameter η_j lies in the smectic plane and it is perpendicular to the tilt vector. b) Top view on the layers. The ellipse now presents the projection of the molecule on the smectic plane.

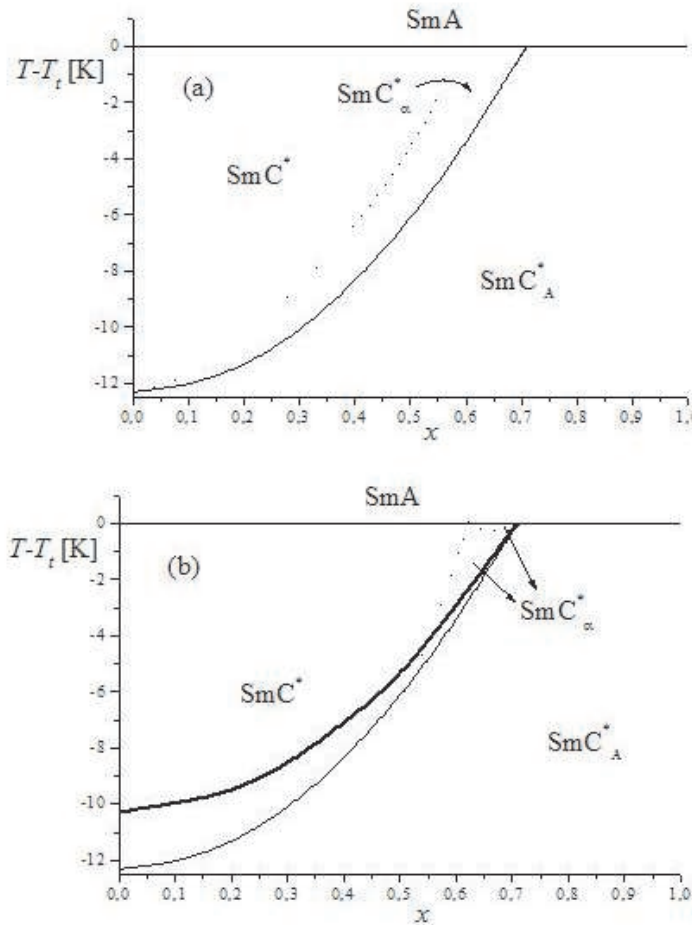


Fig. 3 N. Vaupotic and M. Cepic PRE

Figure 3: Phase diagrams if no flexoelectric coupling is present. a) $b_Q = 0$; without the dotted line: $f_1 = -0.01x$, with the dotted line: $f_1 = -0.05x$. b) $f_1 = -0.05x$; thin dotted and solid line: $b_Q = -1$; thick dotted and solid line: $b_Q = -10$. Solid and dotted lines denote the first order and the second order transitions, respectively. The SmC_α^* phase is designated to the region in which $\alpha > 0.2$. The common set of parameters: $\mu = 0$, $c_p = 4x$, $b = 120$, $a_{10} = -0.4$, $a_{11} = 4$, $b_0 = 2$ and $b_1 = b_0/10$. All the parameters are given in the units of Kelvin. T_t is the transition temperature to the tilted phase.

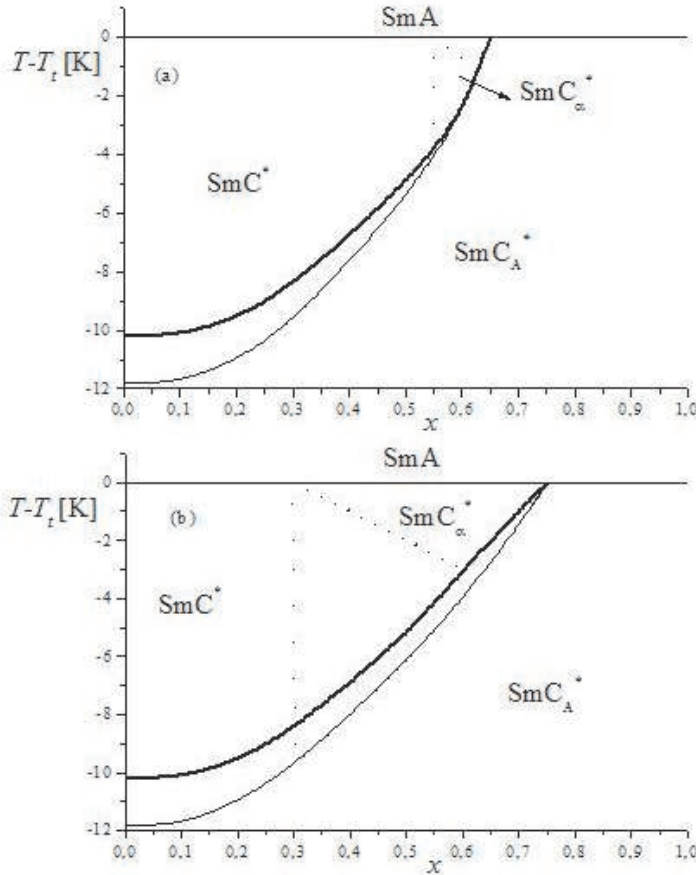


Fig. 4 N. Vaupotic and M. Cepic PRE

Figure 4: Phase diagrams at finite flexoelectric coupling: the effect of the sign of the effective chiral interaction and the quadrupolar coupling. a) $\tilde{f}_1 = -\tilde{f}_2 = 0.06x$; b) $\tilde{f}_1 = \tilde{f}_2 = -0.06x$. Both graphs: thin solid and dotted line: $b_Q = -2$; thick solid and dotted line: $b_Q = -10$. Solid and dotted lines denote the first order and the second order transitions, respectively. The common set of parameters: $\mu = 0.3$, $c_p = 4x$, $b = 120$, $a_{10} = -0.4$, $a_{11} = 4$, $b_0 = 2$ and $b_1 = b_0/10$.

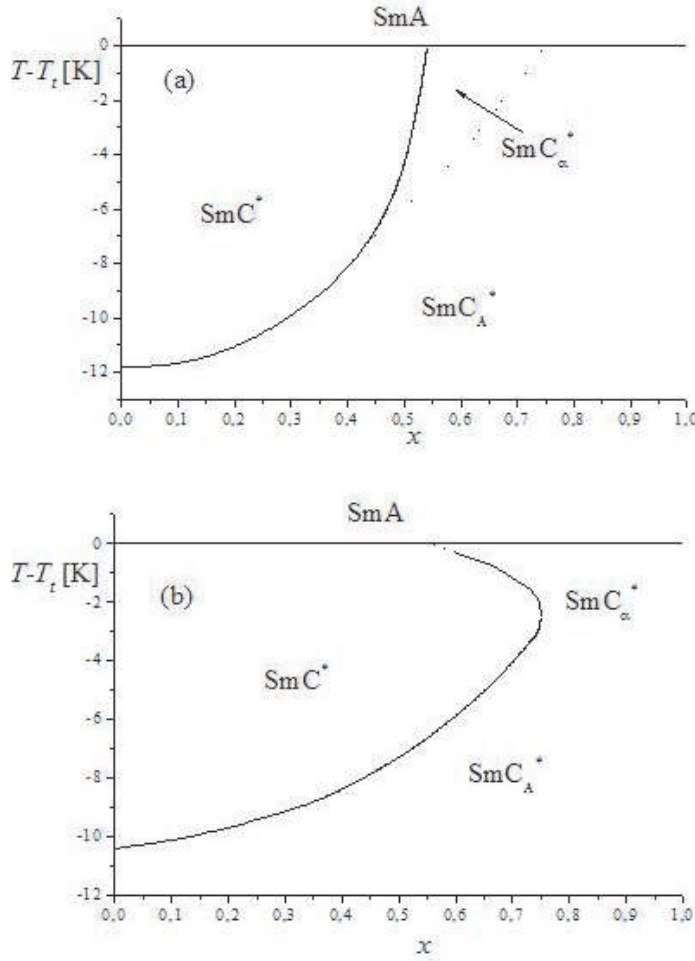


Fig. 5 N. Vaupotic and M. Cepic PRE

Figure 5: Phase diagrams at $\mu = 0.5$, $c_p = -3x$, $\tilde{f}_1 = -0.17x$ and $\tilde{f}_2 = 0.075x$. The rest of the parameters are the same as in Fig. 4. a) $b_Q = -2$ and b) $b_Q = -10$. Solid and dotted lines denote the first order and the second order phase transitions, respectively. The SmC_α^* phase is designated to the region in which $\alpha < 1.5$.

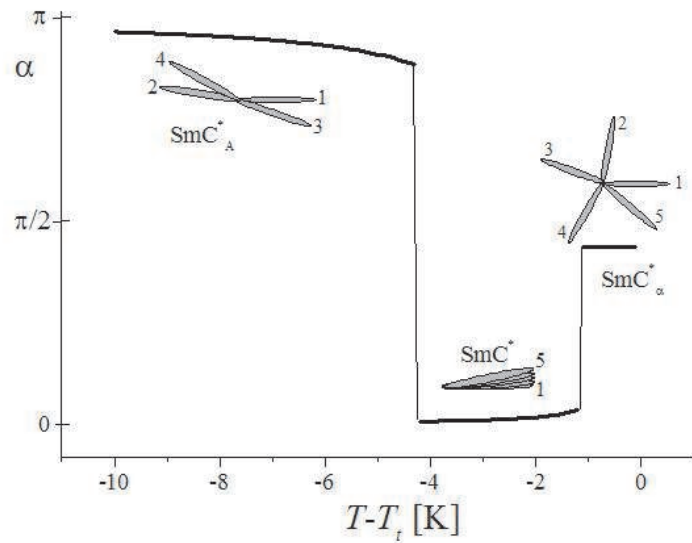


Fig. 6 N. Vaupotic and M. Cepic PRE

Figure 6: Temperature dependence of the phase angle α at $x = 0.7$ for the phase diagram shown in Fig. 5b. At this optical purity all the three clock phases are observed when temperature is reduced below the transition temperature T_t to the tilted phase. All the transitions are of the first order. A schematic diagram (top view on the layers) is shown for each phase. The numbers count the successive layers.